Available online at www.sciencedirect.com
ScienceDirect
International Journal of Heat and Mass Transfer 51 (2008) 3217–3226
International Journal of HEAT and MASS TRANSFER
www.elsevier.com/locate/ijhmt

Inverse design involving combined radiative and turbulent convective heat transfer

A.C. Mossi [a], H.A. Vielmo [a], F.H.R. França [a,*], John R. Howell [b]

[a] Department of Mechanical Engineering, Federal University of Rio Grande do Sul, UFRGS, Rua Sarmento Leite, 425. Centro, CEP: 90050-170 Porto Alegre, RS, Brazil
[b] Department of Mechanical Engineering, The University of Texas at Austin, 1 University Station, C2200 Austin, TX 78712-0292, USA

Received 7 March 2007; received in revised form 14 November 2007

Abstract

This work considers an inverse boundary design problem which involves radiation and convection heat transfer. The objective is finding the heat flux distribution required on heaters located on the top and side walls of a two-dimensional enclosure that satisfies both the temperature and heat flux distributions prescribed on the design surface of the enclosure. A turbulent air flow is generated by a fan located inside the chamber. The problem is described by a system of non-linear, ill-conditioned equations, which is solved by an iterative procedure. The solution are obtained by regularizing the system of equations by means of the TSVD method.

Keywords: Inverse design; Combined heat transfer; Turbulent convection; Thermal radiation; TSVD regularization

1. Introduction

Many industrial processes, from the metallurgy field to the rapid thermal processing of silicon wafers, require controlled heating of materials. For instance, in thermal processing of materials, uniformity of temperature is often required to avoid thermal stresses and allow a better control of several manufacturing processes. This can be achieved only by means of a carefully controlled heat flux on the surface of the processed material, so both the temperature and heat flux are in fact imposed. The thermal designer aims at finding the thermal conditions of the system so that these two conditions are simultaneously satisfied.

In the inverse design approach, the conditions in the unconstrained elements are found directly from the two specifications on the design surface, avoiding the trial-and-error procedure of the forward design. The mathematical model allows the prescription of two conditions in some boundaries while other regions are left unconstrained. For problems that involve thermal radiation heat transfer, this type of formulation is described by a Fredholm integral equation of the first kind, known to result in ill-posed problems that can be solved by means of regularization methods [1] or by optimization. A comprehensive review of steady state inverse design can be found in França et al. [2], and recent contributions on transient inverse design is discussed in Daun et al. [3] and França and Howell [4]. Despite combined heat transfer modes occurring in most of the thermal systems, few inverse solutions are available for this type of problem. França et al. [5] presented an inverse design of a system considering both convection and radiation, but the analysis was limited to a prescribed one-dimensional laminar, parallel flow. While the work proposed a general method for the treatment of the problem, the simplicity of the flow does not permit understanding many aspects of the effect of the convection mechanism in more realistic systems where the flow is turbulent.

This paper considers an inverse boundary design of a two-dimensional rectangular enclosure where the heat

* Corresponding author. Tel.: +55 51 3308 3360; fax: +55 51 3308 3355.
E-mail address: frfranca@mecanica.ufrgs.br (F.H.R. França).

0017-9310/$ - see front matter © 2008 Elsevier Ltd. All rights reserved.
doi:10.1016/j.ijheatmasstransfer.2008.02.001

Nomenclature

$\mathbf{A}$	matrix formed by view factors
$c_{\varepsilon 1}$	constant of the κ–ε equations
$c_{\varepsilon 2}$	constant of the κ–ε equations
c_{μ}	constant of the κ–ε equations
D	design surface
F	view factor
H	heater
k	turbulence kinetic energy, m^2/s^2
L	distance, m
$\bar{p}$	time-average pressure, Pa
Pr_t	turbulent Prandtl number
Q	dimensionless heat flux, $Q = q/\sigma T_{ref}^4$
q_t	total heat flux, W/m^2
q_c	convective heat flux, W/m^2
q_r	radiative heat flux, W/m^2
q_o	radiosity, W/m^2
q_i	irradiation, W/m^2
$q_{prescribed}$	prescribed heat flux, W/m^2
t	dimensionless temperature, $t = T/T_{ref}$
$T_{prescribed}$	prescribed temperature, K
T	temperature, K
$\bar{T}$	time-average temperature, K
$\mathbf{U}$	orthogonal matrix
$\bar{u}$	time-average velocity, m/s
u'	fluctuation velocity, m/s
$\mathbf{V}$	orthogonal matrix
$\bar{v}$	time-average velocity, m/s
v'	fluctuation velocity, m/s
$\mathbf{W}$	matrix formed by singular values
W	insulated wall
$\bar{X}$	time-average field force in the x direction, m/s^2
x	horizontal coordinate
$\bar{Y}$	time-average field force in the y direction, m/s^2
y	vertical coordinate

Greek symbols

α_t	thermal eddy diffusivity, m^2/s
ε	turbulence dissipation rate, m^2/s^3
ε_d	design surface emissivity
ε_h	heater surface emissivity
ε_w	insulated wall surface emissivity
μ	dynamic viscosity, N s/m^2
μ_t	momentum eddy viscosity, N s/m^2
ρ	density, kg/m^3
σ	Stefan–Boltzmann constant, $W/m^2\,K^4$
σ_κ	constant of the κ–ε equations
σ_ε	constant of the κ–ε equations
γ	error, %

Subscripts

jd	design surface element
jh	heating element
jw	insulated wall element

Superscript

T	transpose matrix

transfer is governed by thermal radiation and turbulent convection. The objective is to find the heat input on the heater located on the top and side surfaces of the enclosure so that the temperature and the heat flux imposed on the design surface are both attained. All physical properties are assumed uniform, except the air density, which is temperature dependent to account for buoyancy effects. The surfaces are gray emitters and absorbers. The fluid flow and the diffusive–advective terms of the energy equation are treated numerically by the control volume method, with the turbulent transport being described by the κ–ε model. The radiative terms are treated by the discretization of the surfaces into uniform-sized zones. Due to the different characteristics of the radiation and convection mechanisms, different meshes are used for each one. The central part of the inverse analysis relates the radiation transferred between the heater and the design surface, forming an ill-conditioned system of linear equations on the radiosities of the heater elements. The other terms of the energy equations are incorporated into the problem by an iterative procedure. The ill-conditioned nature of the system is treated by the truncated singular value decomposition (TSVD), a regularization method that also permits the solution of problems having unequal number of unknowns and equations. The proposed methodology is applied to a few example cases to illustrate some typical characteristics of a radiation–convection combined mode inverse design.

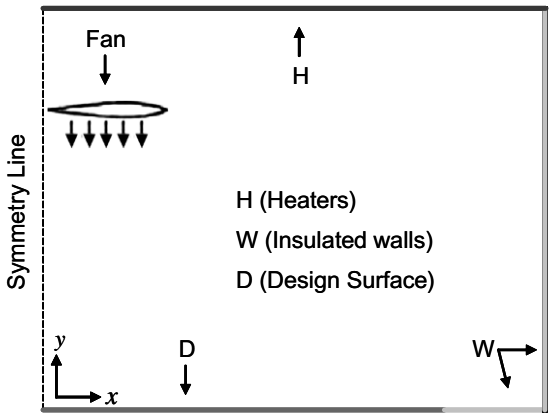

Fig. 1. Schematic of one-half of the two-dimensional enclosure.

2. Physical and mathematical model

Fig. 1 presents a schematic view of the two-dimensional system. The surfaces of the enclosure are assumed as gray and diffuse, an assumption that in general holds as a good approximation for the analysis of thermal processes in furnaces where thermal radiation is mainly in the infrared region of the wavelength spectrum. Due to symmetry, only one-half of the enclosure is shown. The space inside the enclosure is filled with air, a non-participating medium. Heat transfer is governed by thermal radiation exchange between the surfaces and by turbulent convective transfer between the air flow and the surfaces. The design surface is located on the bottom, and the heaters are located on the top and/or side of the enclosure. The remainder of the enclosure is formed by walls that are considered to be insulated from the outside. To reduce the computation effort, only one-half of the enclosure is simulated.

For the numerical simulations, different discretizations of the domain were used for the radiation and convection mechanisms, since in general turbulent convection requires much more grid refinement in the proximity of the surfaces than is necessary for a sufficiently accurate computation of the radiation exchanges. For this reason, while the thermal radiation grid mesh consisted of the division of the walls into equal-sized segments, the convection grid mesh involved non-uniform surface and volume elements, which are based on the hyperbolic functions presented in Davidson [6]. The convection grid mesh is shown in Fig. 2.

The mathematical model of the radiation exchanges between the surfaces relies on the relations for enclosures [7]. The problem is formulated by a system of integral equations, which can be solved numerically by the discretization of the domain into finite size elements. The element indices on the design surface, heater and insulated walls are designated by *jd*, *jh* and *jw*, while the number of elements on these surfaces are designated by JD, JH and JW, respectively. The radiative heat flux on a design surface element *jd* is given by the difference between the radiosity and irradiation (both in W/m^2):

$$q_{r,jd} = q_{o,jd} - q_{i,jd}. \tag{1}$$

The radiosity $q_{o,jd}$ accounts for both emission and reflection from the design surface element. Considering that the temperature and the radiative heat fluxes are specified on the design surface, the radiosity of the design surface element can be readily found from the relation:

$$q_{o,jd} = \sigma T_{jd}^4 - \frac{1-\varepsilon_d}{\varepsilon_d} q_{r,jd}, \tag{2}$$

where T_{jd} is the absolute temperature of design surface element *jd*, in K, σ is the Stefan–Boltzmann constant, equal to 5.67×10^{-8} W/m^2 K^4 and ε_d is the hemispherical emissivity of the design surface. The irradiation $q_{i,jd}$ accounts for all the incident radiative energy on the design surface element, including both emissions and reflections from the other surfaces of the enclosure, and is given by

$$q_{i,jd} = \sum_{jh}^{JH} F_{jd-jh} q_{o,jh} + \sum_{jw}^{JW} F_{jd-jw} q_{o,jw}. \tag{3}$$

In the above equation, F_{jd-jh} and F_{jd-jw} are, respectively, the view factors between elements on the design surface and on the heater, and between elements on the design surface and on the wall; $q_{o,jh}$ and $q_{o,jw}$ are the radiosities of element *jh* on the heater and of element *jw* on the wall, respectively.

As stated before, no thermal condition has been imposed on the heater. At this point, however, it is possible to rearrange Eqs. (1) and (3) to provide an equation for the radiosity of the heater elements:

$$\sum_{jh=1}^{JH} F_{jd-jh} q_{o,jh} = q_{o,jd} - q_{r,jd} - \sum_{jw=1}^{JW} F_{jd-jw} q_{o,jw}. \tag{4}$$

A radiative energy balance on the insulated wall elements leads to an equation for the radiosities $q_{o,jw}$:

$$q_{o,jw} = q_{r,jw} + \sum_{jd=1}^{JD} F_{jw-jd} q_{o,jd} + \sum_{jh=1}^{JH} F_{jw-jh} q_{o,jh} + \sum_{jw^*=1}^{JW} F_{jw-jw^*} q_{o,jw^*}. \tag{5}$$

For the insulated wall elements, the net heat transfer is null, so that the radiative and the convective heat fluxes, $q_{r,jw}$ and $q_{c,jw}$, cancel each other, that is

$$q_{r,jw} + q_{c,jw} = 0. \tag{6}$$

Finally the radiation formulation is completed by setting a relation for the net radiative heat flux on the heater elements:

$$q_{r,jh} = q_{o,jh} - \sum_{jd=1}^{JD} F_{jh-jd} q_{o,jd} - \sum_{jw=1}^{JW} F_{jh-jw} q_{o,jw} - \sum_{jh^*=1}^{JW} F_{jh-jh^*} q_{o,jh^*}. \tag{7}$$

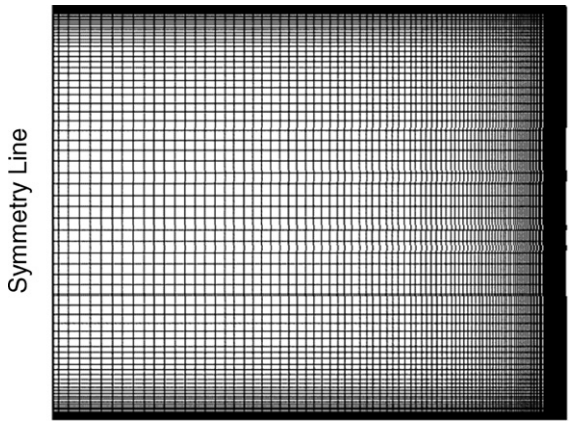

Fig. 2. Discretization of the enclosure for the numerical solution of the convection heat transfer equations. The thermal radiation grid mesh consisted of the division of the walls into equal segments.

In Eq. (5), the last term on the right-hand side arises from the fact that an insulated wall element *jw* can "see" another insulated wall element *jw**, as shown in Fig. 1. The same applies to the last term of Eq. (7) regarding the heater elements *jh* and *jh**.

The computation of the heat transfer between the air and the surfaces requires the solution of the fluid flow and temperature field in the air. The fluid flow can be solved by the time-averaged continuity and momentum equations in the x and y direction, as given by Bejan [8] and Launder and Spalding [9]:

$$\frac{\partial(\rho\bar{u})}{\partial x}+\frac{\partial(\rho\bar{v})}{\partial y}=0, \tag{8}$$

$$\bar{u}\frac{\partial\bar{u}}{\partial x}+\bar{v}\frac{\partial\bar{u}}{\partial y}=\frac{1}{\rho}\frac{\partial\bar{p}}{\partial x}+\frac{\mu}{\rho}\left(\frac{\partial^2\bar{u}}{\partial x^2}+\frac{\partial^2\bar{u}}{\partial y^2}\right)-\left(\frac{\partial(\overline{u'^2})}{\partial x}+\frac{\partial(\overline{u'v'})}{\partial y}\right), \tag{9}$$

$$\bar{u}\frac{\partial\bar{v}}{\partial x}+\bar{v}\frac{\partial\bar{v}}{\partial y}=\bar{Y}-\frac{1}{\rho}\frac{\partial\bar{p}}{\partial y}+\frac{\mu}{\rho}\left(\frac{\partial^2\bar{v}}{\partial x^2}+\frac{\partial^2\bar{v}}{\partial y^2}\right)-\left(\frac{\partial(\overline{u'v'})}{\partial x}+\frac{\partial(\overline{v'^2})}{\partial y}\right). \tag{10}$$

The term $\bar{Y}$ in Eq. (10) accounts for the buoyancy force, given by the product between the density and the gravitational acceleration,ρg, where the temperature dependence of the density is given by

$$\rho(T)=1.09\times10^{-2}-2.05\times10^{-3}T+1.85\times10^{-6}T^2-6.01\times10^{-10}T^3 \tag{11}$$

in which the density is in kg/m^3 and the temperature is in K. For the conditions considered in the paper, natural convection is of minor importance in relation to forced convection, and could be omitted from the analysis without noticeable effect on the results. The momentum transport of the turbulent eddies is modeled by the Boussinesq hypothesis, given by

$$-\overline{u'v'}=\frac{\mu_t}{\rho}\frac{\partial\bar{u}}{\partial y}. \tag{12}$$

In the κ–ε turbulence model, the momentum eddy viscosity, $\nu_t=\mu_t/\rho$, is computed from the relation $c_\mu\kappa^2/\varepsilon$, where the values of κ and ε come directly from the differential transport equations for the turbulence kinetic energy and turbulence dissipation rate:

$$\bar{u}\frac{\partial\kappa}{\partial x}+\bar{v}\frac{\partial\kappa}{\partial y}=\left(\frac{\mu}{\rho}+\frac{\mu_t}{\rho\sigma_\kappa}\right)\left(\frac{\partial^2\kappa}{\partial x^2}+\frac{\partial^2\kappa}{\partial y^2}\right)+\frac{\mu_t}{\rho}\left(\frac{\partial\bar{u}}{\partial y}+\frac{\partial\bar{v}}{\partial x}\right)\left(\frac{\partial\bar{u}}{\partial y}\right)-\varepsilon, \tag{13}$$

$$\bar{u}\frac{\partial\varepsilon}{\partial x}+\bar{v}\frac{\partial\varepsilon}{\partial y}=\left(\frac{\mu}{\rho}+\frac{\mu_t}{\rho\sigma_\varepsilon}\right)\left(\frac{\partial^2\varepsilon}{\partial x^2}+\frac{\partial^2\varepsilon}{\partial y^2}\right)+c_{\varepsilon1}\frac{\mu_t}{\rho}\frac{\varepsilon}{\kappa}\left(\frac{\partial\bar{u}}{\partial y}+\frac{\partial\bar{v}}{\partial x}\right)\left(\frac{\partial\bar{u}}{\partial y}\right)-c_{\varepsilon2}\frac{\varepsilon^2}{\kappa}, \tag{14}$$

where $c_\mu=0.09$, $c_{\varepsilon1}=1.44$, $c_{\varepsilon2}=1.92$, $\sigma_\varepsilon=1.3$ and $\sigma_\kappa=1$.

The energy equation is given by

$$\bar{u}\frac{\partial\bar{T}}{\partial x}+\bar{v}\frac{\partial\bar{T}}{\partial y}=\frac{\mu_t}{Pr_t}\left(\frac{\partial^2\bar{T}}{\partial x^2}+\frac{\partial^2\bar{T}}{\partial y^2}\right), \tag{15}$$

where Pr_t is the turbulent Prandtl number, which relates the momentum and the thermal eddy viscosities, ν_t/α_t, and is taken as equal to 0.9 [10]. Although turbulence is an intrinsically three-dimensional, asymmetrical phenomenon, the two-dimensional conservation equations above allow considering the major effects of turbulence in a time-average sense, which suffices for the objectives of this analysis, which is centered in the inverse methodology.

Boundary conditions are required for all the conservation equations. On the walls, the non-slip and impermeability conditions are imposed, so $u=v=0$, and the air temperature is set equal to the wall temperature. In the symmetry line, on the left, all gradients in the x-direction are null, $\partial(\,)/\partial x=0$. To account for the effect of the fan, in the control volumes occupying the position where the fan blades are located, a uniform velocity v_o is prescribed.

The finite volume method was used to solve Eqs. (8)–(15). The advective terms of Eqs. (9), (10), (13), (14) and (15) were solved by the power-law interpolation; the SIMPLE (semi implicit method for pressure linked equations) algorithm was used to link the pressure–velocity field; and the linear system of equations generated by the finite volume method was solved by the TDMA (tri-diagonal matrix algorithm).

3. Solution procedure

3.1. Regularization of the system of equations

In inverse analysis of purely radiative heat transfer processes, the prescribed heat flux on the design surface is equal to the radiative heat flux. This is the starting point of the inverse solution, for the radiosity in the design surface can be directly computed from Eq. (2) with the known temperature and radiative heat flux. In combined heat transfer mode, the prescribed (total) heat flux is a combination of the radiation and convection mechanisms:

$$q_{t,jd}=q_{r,jd}+q_{c,jd}. \tag{16}$$

Therefore, the radiative heat flux on the design surface is no longer the same as the total heat flux; in fact both the radiative and the convective heat flux are unknown, and need to be found from the solution of the governing equations.

To allow the use of the pure radiative inverse design methodology, an iterative procedure is proposed in which the convective flux is initially guessed followed by a radiative heat flux computed from Eq. (16). Next, the radiosities of the design surface elements are determined from the application of Eq. (2). The energy balance for the design surface is taken to form a system of linear equations to

solve for the unknown radiosities of the heater elements, as given by Eq. (4). This system has two challenging aspects. First, the number of equations is equal to the number of design surface elements, JD, while the number of unknowns is equal to the number of heater elements, JH. Therefore, unless JD and JH are equal, the numbers of equations and of unknowns are not the same. Secondly, the system is expected to be ill-conditioned due to its inverse nature. The application of conventional methods of matrix inversion inevitably leads to a solution vector whose components present steep oscillations between positive and negative numbers, which is not physically acceptable since the radiosities must be positive numbers.

The above two difficulties can be dealt with the application of so-called regularization methods. Such methods impose additional constraints to the original problem to smooth the solution vector, although at the expense of introducing an error into the solution. Well known methods include techniques based on singular value decomposition (SVD), schemes using Tikhonov regularization, and conjugate gradient regularization methods.

In this work, the truncated singular value decomposition (TSVD) was the selected method. First, matrix **A**, corresponding to the set of Eq. (4), and whose components are the view factors F_{jd-jh}, is singularly decomposed into three matrices:

$$\mathbf{A} = \mathbf{U}\mathbf{W}\mathbf{V}^{\mathrm{T}}, \tag{17}$$

where **U** and **V** are orthogonal matrices, and **W** is a diagonal matrix formed of the singular values w_j. The solution vector **x**, which is formed by the radiosities of the heater elements, is computed by

$$\mathbf{x} = \sum_{j=1}^{\mathrm{JH}} \left(\frac{b_k \cdot u_{kj}}{w_j} \right) \mathbf{v}_j. \tag{18}$$

In ill-posed problems, the singular values w_j decay continuously to very small values. Since they are in the dominator of Eq. (18), this results in components of **x** with very large absolute numbers. However, the smaller is the singular value w_j, the closer is the corresponding vector v_j to the null-space of **A**. In other words, the terms related to the smaller singular values can be eliminated from Eq. (18), without introducing a large error to the solution. This is the main idea of the TSVD: only the terms related to the pth largest singular values are kept in Eq. (18), instead of all JH terms. The solution is the vector **x** with the smallest norm subjected to minimum deviation $|\mathbf{A} \cdot \mathbf{x} - \mathbf{b}|$. Another important feature of the TSVD method is that it can also be applied to the case where the numbers of unknowns and equations are not the same, as will be discussed in Section 4.

3.2. Solution strategy

The first step consists of dividing the computational domain into control volumes for the solution of the convection process, and dividing the surfaces into equal-size areas for the solution of the radiation exchange relations. On the design surface, both the temperature and the total heat flux are prescribed. The solution is based on the following steps:

1. The convective heat fluxes on the design surface and insulated wall elements, $q_{c,jd}$ and $q_{c,jw}$, are guessed (starting with $q_{c,jd} = 0$ and $q_{c,jw} = 0$), and the radiative heat fluxes on the design surface and insulated wall elements, and, are computed from Eqs. (16) and (6), respectively.
2. The radiosities of the insulated wall elements, $q_{o,jw}$, are guessed (starting with $q_{o,jw} = 0$).
3. The radiosities of the design surface elements, $q_{o,jd}$, are computed from Eq. (2). Eq. (4) is written for all JD design surface elements to solve for the JH radiosities of the heater elements, $q_{o,jh}$. The system of equations is solved for $q_{o,jh}$, and the radiosities $q_{o,jw}$ are recalculated from the application of Eq. (5) to the JW wall elements (forming a well-conditioned system of linear equations with JH unknowns and equations).
4. Step 3 is repeated, redoing the calculations with the new values of $q_{o,jw}$ until the radiosities $q_{o,jh}$ converge with a maximum relative deviation of 10^{-6} between the last two iterations.
5. Eq. (7) is applied to the JH heater elements to find the net radiative heat fluxes, $q_{r,jh}$, on the heater elements. The application of the radiative relations also allows the determination of the temperature distribution on the heater and on the insulated walls. At this point, the inverse solution is complete for the imposed values of $q_{r,jd}$, which was computed from the guessed values of $q_{c,jd}$ (in Step 1).
6. With the obtained temperature distribution on the enclosure surfaces, the convective governing equations given by (8)–(15) provide a means for determining the convective heat fluxes on all surfaces of the enclosure.
7. Step 1 is repeated, redoing the calculations with the new values of $q_{c,jd}$ and until $q_{r,jd}$ and converge with a maximum relative deviation of 10^{-6} between the last two iterations.
8. After the convergence of the numerical solution, the total heat input in the heater elements, $q_{t,jh}$, the information that is sought by the inverse analysis, is computed by

$$q_{t,jh} = q_{r,jh} + q_{c,jh} \tag{19}$$

Combined radiation–convection heat transfer problems are known to be generally difficult to converge. To allow convergence using the proposed method, the convective heat fluxes $q_{c,jd}$ were under-relaxed in Step 7 with a factor of 0.05. The insulated wall element radiosities, $q_{o,jw}$, are under-relaxed in Step 3 with a factor of 0.1.

3.3. Verification of the solution

The application of TSVD regularization inevitably introduces an error to the solution, since only $p <$ JH terms

are kept in the series of Eq. (18). Verification of the inverse solution is straightforward. With the obtained total heat fluxes on the heaters, a forward problem in which the temperatures on the design surface elements and the total heat fluxes on the heaters and insulated walls are known is run to find the total heat flux on the design surface, $q_{t,jd}$, which can be compared with the prescribed heat flux, $q_{\text{prescribed}}$, by

$$\gamma_{\max} = \max_{jd} \left| \frac{q_{t,jd} - q_{\text{prescribed}}}{q_{\text{prescribed}}} \right|. \tag{20}$$

4. Results and discussion

The system considered in this work is a two-dimensional enclosure as shown in the general schematic of Fig. 1. Taking advantage of the symmetry, only one-half of the domain is solved. The dimensions of the enclosure in Fig. 1 are $L = 0.70$ m and $H = 0.56$ m. Although the present analysis allows the specification of different total hemispherical emissivities for the surfaces, it is considered that their values for the design surface, the heater and the walls are the same and equal to $\varepsilon_d = \varepsilon_h = \varepsilon_w = 0.8$. It is specified that the temperature and total heat flux on the design surface are respectively $T_{\text{prescribed}} = 673$ K and $q_{\text{prescribed}} = -3.220 \times 10^3$ W/m^2. The negative sign follows from the convention that power added to a system is positive. The results are presented in dimensionless form: the dimensionless temperature and heat flux are defined by $t = T/T_{\text{ref}}$ and $Q = q/\sigma T_{\text{ref}}^4$, where the reference temperature is $T_{\text{ref}} = 1173$ K. Therefore, for the design surface, the prescribed conditions are $t_{\text{prescribed}} = 0.574$ and $q_{\text{prescribed}} = -0.3$. A few solutions for the heat flux distribution on the heaters are presented next.

Fig. 3 presents Case 1. It is considered that the heater occupies the entire extension of the top surface, while the right-hand surface remains insulated. The design surface is located on the bottom of the enclosure, but is kept at some distance from the right corner. Previous studies (França et al., 2003) have shown that the portion of the design surface close to the corner is much less affected by the heater than by the insulated surface itself. For this reason, placing design surfaces on the right side, near the insulated wall, would make it much more difficult, if not impossible, to find a satisfactory solution on the heater. The radiation mesh was divided into 50 and 40 uniform-sized elements in the x and y directions, so that the dimensionless sizes of the surface elements were $\Delta x/L = \Delta y/L = 0.02$. For the convection part, shown in Fig. 2, the mesh was divided into 120 and 90 elements in the x and y directions, respectively. To capture the steep variations of temperature and fluid velocities close to the surfaces, as expected in turbulent flows, a non-uniform mesh was adopted using the same hyperbolic functions presented in Davidson [6], with an aspect ratio of 2.5 in both directions. For all cases presented in this paper, the solutions proved to be satisfactorily grid independent for these two mesh configurations.

For a better understanding of the effect of including the convective heat transfer in the inverse analysis, a purely radiative enclosure is first solved, in which no flow is provided by the fan and free convection is neglected. In this case, the total radiative heat flux is equal to the total heat flux. The problem is modeled by a system of linear equations, as described in Sections 2 and 3. For the pure radiation problem the numbers of computational area elements on the design surface and on the heater are JD = 36 and JH = 50, respectively. For this choice of design surface and heater elements, the number of equations (equal to JD) and the number of unknowns (equal to JH) are not the same, a situation that typically occurs in inverse design problems. The application of the TSVD regularization to the system of equations results in the singular values shown in Fig. 4 with the label Case 1. A total of JH = 50 singular values are generated, but only the first 36 values (the same

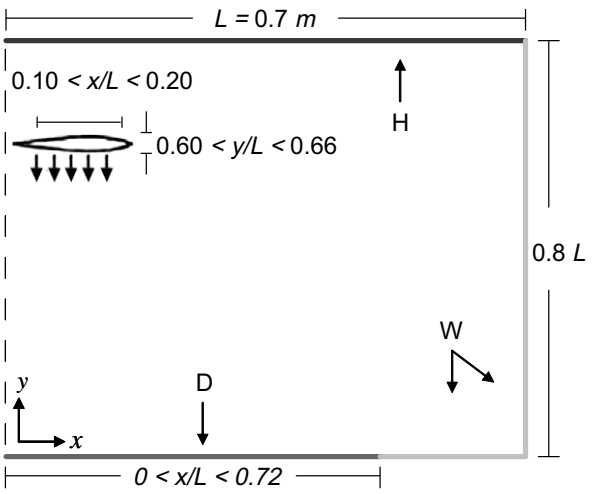

Fig. 3. Design surface and heater configurations for Case 1.

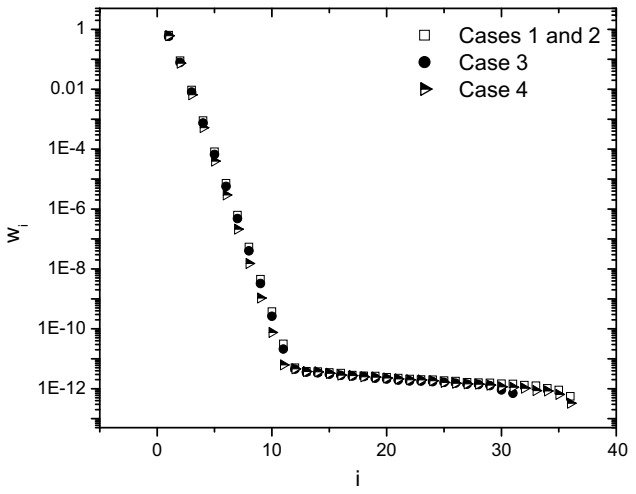

Fig. 4. Singular values of matrix A for the different solution cases.

as the number of equations, JD) are non-zero, which are the ones shown in Fig. 4. The steep decay of the singular values indicates the ill-conditioned nature of the system of equations. Keeping all the terms of the series of Eq. (18) results in negative values for the radiosities $q_{o,jh}$, a non-physically acceptable solution. The TSVD regularization eliminates the high-order terms of the series to smooth the solution and recover positive values for the radiosities $q_{o,jh}$. Fig. 5 presents the total heat flux on the heater elements when keeping only two ($p = 2$) and three ($p = 3$) terms of the series. Setting a larger number of terms resulted in negative heat fluxes (a non-practical solution) or negative radiosities (a physically unacceptable solution) on the heaters. The resulting heat fluxes on the design surface, computed from the procedure described in Section 3.3, are also shown in the figure for the solutions with $p = 2$ and $p = 3$. As seen, despite eliminating most of the terms of the series of Eq. (18), it was possible to obtain different solutions for the heater that were both capable of satisfying the desired heat flux on the design surface with a small error, as given by Eq. (20): for $p = 2$, $\gamma_{max} = 0.84\%$; for $p = 3$, $\gamma_{max} = 0.10\%$. Fig. 5 also shows the heat flux on the insulated portion of the bottom surface, which was set equal to zero.

In the above case, the total heat fluxes on the heater and on the design surfaces are solely radiative, since convection was neglected. The more complex case of a coupled radiation–convection problem is now discussed. It is assumed that the fan is operated to generate a typical air flow velocity of 4 m/s, normal to the cross-sectional area of the fan (Fig. 3). The proposed combined mode inverse solution procedure described in Section 3 was applied. Keeping the same heater and design surface configurations of Fig. 3, the singular values are the same as for the purely radiative problem, labeled as Case 1.

In the presence of flow, all attempts of recovering an acceptable solution for the heat flux on the heater failed for this configuration. Even after reducing the number of terms in the series of Eq. (18), it was not possible to avoid negative values for the radiosities on the heater elements. A close analysis revealed that the origin of the difficulty was linked to the stagnation region that exists in the portion of the design surface that is close to the symmetry line. The convective heat transfer in this region was significantly higher than in the other regions of the design surface. Since the total heat flux is prescribed to be uniform, it follows from Eq. (16) that the radiative heat flux on the design surface in the region close to the symmetry line had to be considerably smaller than in the other regions of the design surface, a restriction that made the solution for the heat flux distribution on the heater unviable. This illustrates one characteristic of inverse design: Just specifying conditions on the design surface does not guarantee that an useful solution can be found.

As an attempt to avoid the above difficulty, a new proposition for the design surface was considered, as shown in Fig. 6. In this case, only the temperature condition was prescribed on the portion of the design surface close to the symmetry line (where $x/L \leqslant 0.10$), while the heat flux was left unconstrained, and will be determined from the inverse solution of the heater that will lead to uniformity of temperature and heat flux on the main portion of the design surface ($0.10 \leqslant x/L \leqslant 0.72$). Since the size of the design surface was reduced, keeping the same grid resolution, the number of elements on the design surface was reduced to JD = 31, the same as the number of equations of the system of equations. The singular values of the system are shown in Fig. 4 under label Case 3. Only the 31 non-zero singular values (from the total of 50) are shown in the figure. In this case, it was only possible to recover a physically acceptable solution (that is, positive radiosities on the heater elements) keeping two terms in the series of Eq. (18), $p = 2$. The solution for the total heat distribution on the heater is shown in Fig. 7. The figure also presents the radiative and the convective heat flux distributions. As seen, for

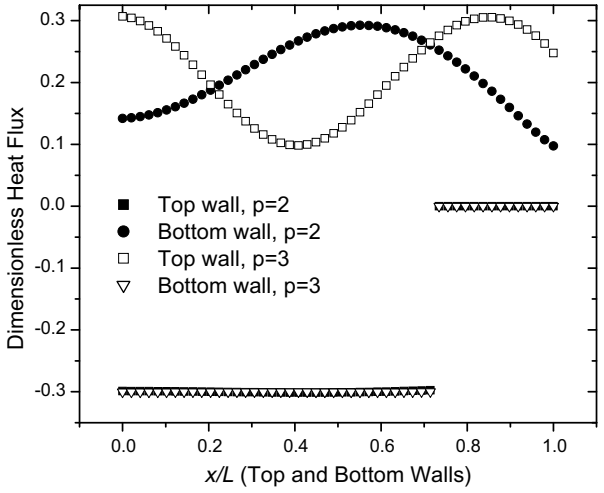

Fig. 5. Total (radiative) flux distributions on the top and bottom surfaces for Case 1 for different regularization parameters p.

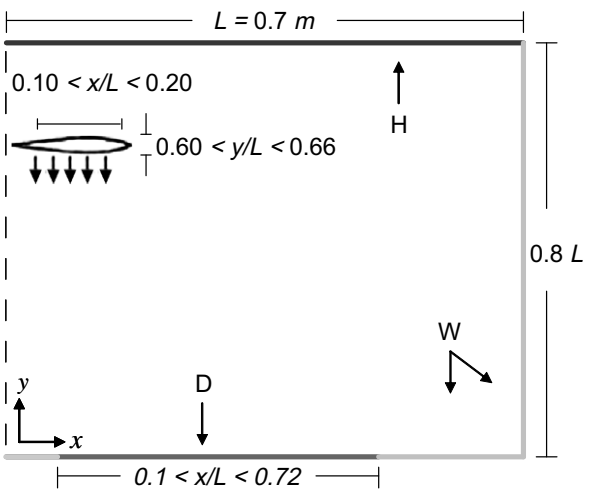

Fig. 6. Design surface and heater configurations for Case 3.

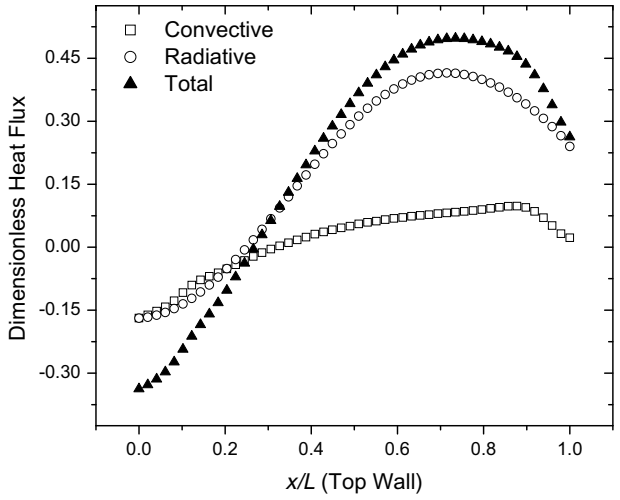

Fig. 7. Total, radiative and convective heat flux distributions on the heater for Case 3.

these conditions, the heat flux on the heater is dominated by thermal radiation, although the convection heat transfer is still an important mechanism to be considered. While the solution is physically acceptable, in the sense that the radiosities of the heater elements are positive, it is not practical, since the total heat flux is negative close to the symmetry line, a result that is not acceptable for a heater design. Despite its non-practicality, it is worth investigating the resulting heat flux on the design surface, which is shown in Fig. 8. This heat flux is obtained by imposing the total heat flux presented in Fig. 7 as the boundary condition on the heater, and then running a forward solution in which the uniform temperature is the sole condition prescribed on the design surface. As seen, the absolute value of the convective heat flux on the design surface increases towards the symmetry; in turn, the radiative heat flux has to decrease to maintain the uniform total heat flux that was imposed. Considering the entire extension of the design surface, the average and maximum errors of the inverse solution were 2.1% and 5.3%.

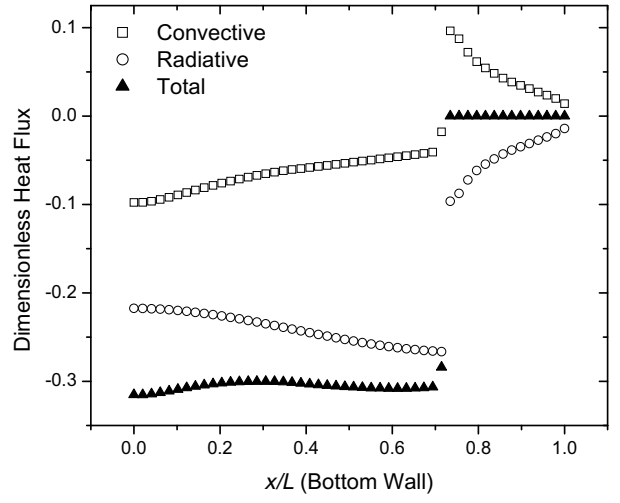

Fig. 8. Total, radiative and convective heat flux distributions on the bottom surface for Case 3.

Other heater configurations, placed both on the top and side walls have been attempted, but failed to provide a completely satisfactory solution for a heater configuration that could provide uniformity of temperature and heat flux on the design surface. A possible explanation for this difficulty is related to the fact that the radiosities of the heating elements converged to solutions with steep oscillations between positive and negative values even after regularization, instead of a smooth solution with positive numbers only. On the other hand, when one imposes a smooth solution for the radiosities, the radiative heat flux tends to be higher on the center of the design surface for a rectangular configuration. However, with the fan blowing directly towards the center of the design surface, the high convective heat flux requires the radiative flux (in absolute values) to be lower in this region, as seen in Fig. 8, which is therefore against the expected behavior for a smooth solution for the radiosities. This suggests that the proposed configuration of the fan, shown in Fig. 3, is not a good design configuration. Fig. 9 shows that the air is blown directly towards the center of the design surface, leading to a high convective heat flux in the center, and requiring the radiative heat flux to be lower in this portion, a condition that is more difficult to attain.

To overcome this difficulty, other flow field configurations can be attempted. For instance, Fig. 10 shows a configuration in which the fan is positioned with the axis in the horizontal position. While this configuration is less common than the one shown in Fig. 3, it will serve as an indication of the effect of the flow pattern on the inverse design. Aiming at an improvement of the solution with respect to Case 3, both uniform temperature and heat flux are again imposed in the entire extension of the design solution. As a first attempt, the heater covered the entire extension of the upper surface. For this case, although it was possible to recover a physically acceptable solution (that is, the radiosities of the heating elements being all positive), the total heat flux on some of the heater elements close to surface 2

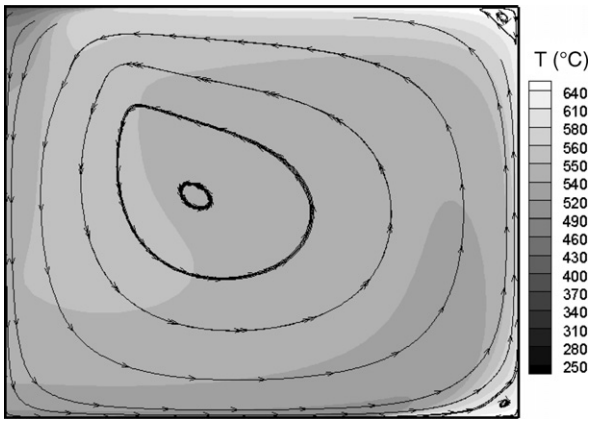

Fig. 9. Air flow streamlines and isotherms for the configuration of Case 3.

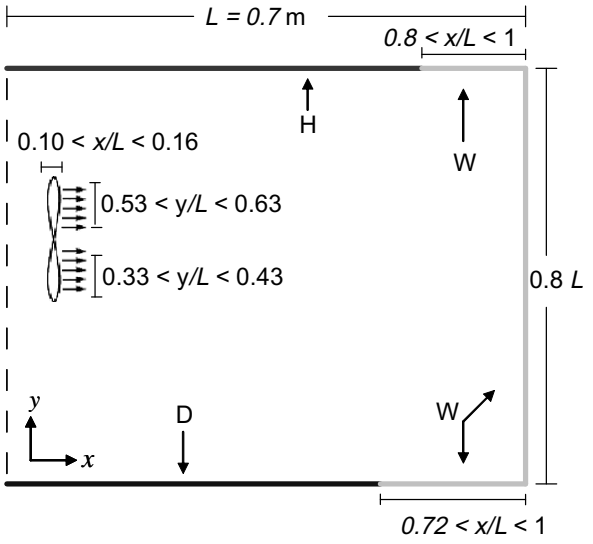

Fig. 10. Design surface and heater configurations for Case 4.

were negative, which is not a practical solution. For this reason, another heater configuration was proposed as shown in Fig. 10. In this case, the heater does not cover the entire extension of the upper surface; to avoid negative heat fluxes on the heating elements close surface 2 ($0.8 \leqslant x/L \leqslant 1.0$), this portion was left insulated.

Fig. 11 presents the heat flux distribution on the upper surface as the result of the inverse solution using $p = 2$. As seen, the required heat input on the heater to satisfy the prescribed uniform temperature and heat flux on the design surface is positive in its entire extension, which makes it a viable solution. The heat transfer is dominated by thermal radiation, although convection is still an important mechanism. Fig. 11 shows that the heat transfer on the left part of the upper surface is null, with the radiation and convection canceling each other. Fig. 12 shows the resulting heat flux on the bottom surface. On the design surface,

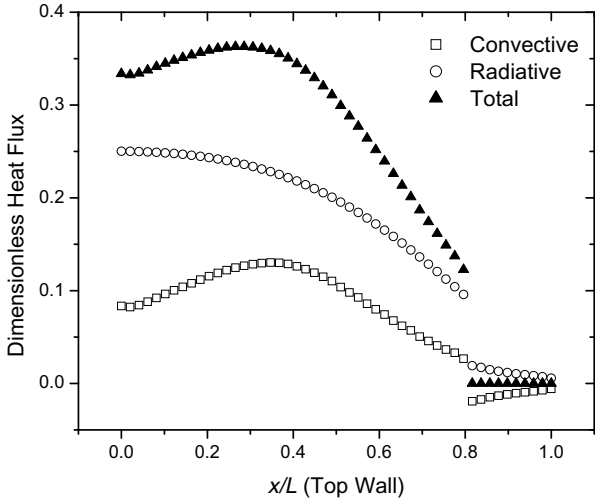

Fig. 11. Total, radiative and convective heat flux distributions on the heater for Case 4.

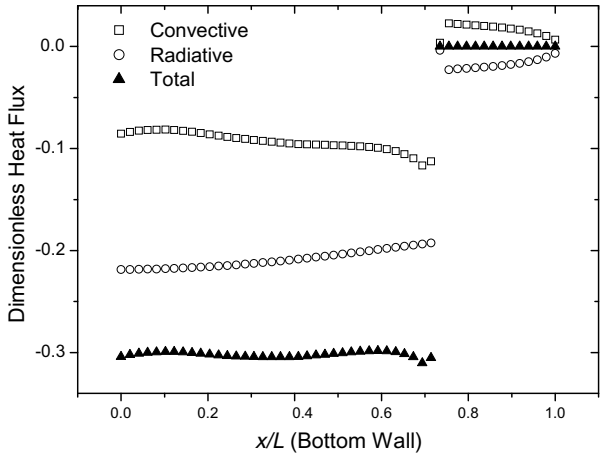

Fig. 12. Total, radiative and convective heat flux distributions on the bottom surface for Case 4.

the total heat flux is close to the specified value of -0.3 with average and maximum errors of 0.83% and 3.43%, respectively. The major contribution of the heat flux is due to thermal radiation, which in this case shows the maximum absolute value in the center of the design surface ($x = 0$). The inversion of the trend in comparison with the situation in Case 3 (Fig. 8) may be the main reason for the inverse analysis to be able to recover a satisfactory solution. The placement of the fans with the axis in the horizontal direction caused an important modification on the air flow pattern. This is shown in Fig. 13. The flow is divided into two major cells, where the largest one is located on the lower part of the enclosure and circulates air from the right portion of the upper surface, where the temperature is not the highest, to the design surface. This is the opposite of the situation found in the configuration of Case 3 (shown in Fig. 9).

A final comment is left for the simplifications that were adopted for modeling the fan. First, partial blocking of radiation between the surfaces by the blades was neglected. In addition, fluid flows generated by fans are three-dimen-

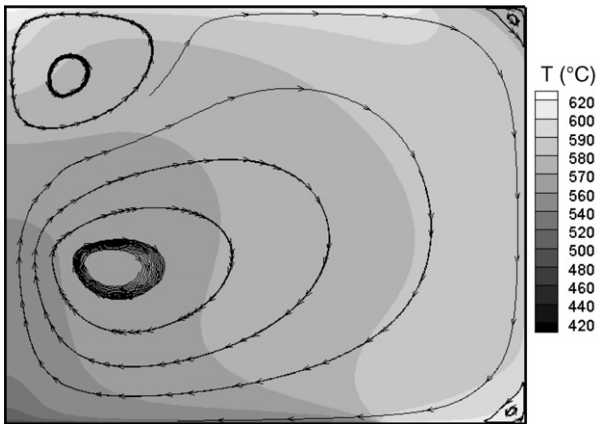

Fig. 13. Air flow streamlines and isotherms for the configuration of Case 4.

sional, not two-dimensional. While considering these two effects would add a great deal of difficulty to the problem and would require a detailed specification of the geometry of the fan blades, it would not change the basic structure of the equations that are inversely solved in the present methodology. For instance, the partial blocking could be accounted for by simply modifying the exchange factors that were obtained for the case without blocking. For this reason, the proposed inverse methodology, outlined in Section 3, is not constrained by the simplifications that have been adopted in the present solution.

5. Conclusions

This paper presented the application of the inverse design technique to determine the power input in the heater of a two-dimensional convective–radiative oven to attain uniformity of temperature and heat flux on the design surface. The central part of the inverse analysis was assembled to relate the heaters directly to the design surface. This led to an ill-conditioned system of linear equations on the heater elements radiosities. Reflections of radiative energy from the insulated walls and the heat transferred from the turbulent air flow were incorporated into the formulation by an iterative procedure. The resulting system of equations was ill-conditioned and has a different number of equations and unknowns. The solution were obtained by regularizing the system using the truncated singular value decomposition (TSVD).

The proposed methodology was applied to a few example cases to demonstrate some typical characteristics of a combined mode inverse design. The first case consisted of a purely radiative enclosure. In this case, regularized solutions were obtained that satisfied the prescribed heat flux with an error less than 1.0%. The cases considering combined radiation–convection heat transfer proved to be considerably more difficult. For the first proposed configuration, with the fan axis located along the symmetry line and blowing air directly to the center of the design surface caused the inverse solution to fail, the main reason being attributed to the relatively low radiative heat flux on the center of the design surface. In an attempt to overcome this difficulty, a second configuration was proposed in which the fans had their axis oriented parallel to the design surface, generating a flow pattern that did not cause direct blowing of high temperature air on the center of the design surface. This configuration allowed obtaining a practical solution for the heater.

Even with the difficulty in extracting physically meaningful results for some of the proposed cases, there is a clear benefit in formulating this design problem in an inverse sense. There was added insight into the reasons why some problems failed which may not have been evident from a purely forward posed design formulation. The insights that are available in posing design problems in an inverse sense cannot be over-emphasized, in particular for difficult problems where the problem statement and associated physics are inherently non-invertible (i.e., having no physical forward equivalent). The results presented in this paper cover only a few examples of the many geometric configurations of the heater that are possible, both in terms of size and position. Another important advance in the research would be establishing a methodology to obtain the best configuration for the heater positions, which may be attempted using optimization techniques.

Acknowledgments

The authors thank CAPES (Brazil) for the support under the Program CAPES/UT-AUSTIN, No. 06/02, as well as the University of Texas Advanced Manufacturing Center.

References

[1] P.C. Hansen, Rank-Deficient and Discrete Ill-Posed Problems: Numerical Aspects of Linear Inversion, SIAM Monographs on Mathematical Modeling and Computation, Philadelphia, 1990.
[2] F. França, J. Howell, O. Ezekoye, J.C. Morales, Inverse design of thermal systems, Adv. Heat Transfer 36 (2002) 1–110.
[3] K. Daun, F. França, M. Larsen, G. Leduc, J.R. Howell, Comparison methods for inverse design of radiant enclosures, J. Heat Transfer 259 (2006) 269–282.
[4] F. França, J. Howell, Transient inverse design of radiative enclosures for thermal processing of materials, Inv. Prob. Sci. Eng. 14 (4) (2006) 1–14.
[5] F. França, O. Ezekoye, J. Howell, Inverse boundary design combining radiation and convection heat transfer, J. Heat Transfer 123 (2001) 884–891.
[6] L. Davidson, Second order corrections of the k–ε model to account for non-isotropic effects due to buoyancy, Int. J. Heat Mass Transfer 33 (1990) 2599–2608.
[7] R. Siegel, J.R. Howell, Thermal Radiation Heat Transfer, fourth ed., Taylor and Francis, New York, 2002.
[8] A. Bejan, Convection Heat Transfer, second ed., John Wiley and Sons, New York, 1995.
[9] B.E. Launder, D.B. Spalding, The numerical computation of turbulent flow, Comput. Meth. Appl. Mech. Eng. 3 (1974) 269.
[10] W.M. Kays, M.E. Crawford, Convective Heat and Mass Transfer, McGraw-Hill, New York, 1993.